ACS APPLIED MATERIALS & INTERFACES

Research Article

www.acsami.org

Reduced Graphene Oxide/Mesoporous TiO_2 Nanocomposite Based Perovskite Solar Cells

Gill Sang Han,[†,‡,#] Young Hyun Song,[†,#] Young Un Jin,[†] Jin-Wook Lee,[§] Nam-Gyu Park,[§] Bong Kyun Kang,[†] Jung-Kun Lee,[‡] In Sun Cho,[*,∥] Dae Ho Yoon,[*,†,⊥] and Hyun Suk Jung[*,†]

[†]School of Advanced Materials Science & Engineering, Sungkyunkwan University, Suwon 440-746, Republic of Korea

[‡]Department of Mechanical Engineering and Materials Science, University of Pittsburgh, Pittsburgh, Pennsylvania 15261, United States

[§]School of Chemical Engineering and Department of Energy Science, Sungkyunkwan University, Suwon, 440-746, Korea

[∥]Department of Materials Science and Engineering & Energy Systems Research, Ajou University, Suwon 443-749, Korea

[⊥]SKKU Advanced Institute of Nanotechnology (SAINT), Sungkyunkwan University, Suwon 440-746, Korea

Supporting Information

ABSTRACT: We report on reduced graphene oxide (rGO)/mesoporous (mp)-TiO_2 nanocomposite based mesostructured perovskite solar cells that show an improved electron transport property owing to the reduced interfacial resistance. The amount of rGO added to the TiO_2 nanoparticles electron transport layer was optimized, and their impacts on film resistivity, electron diffusion, recombination time, and photovoltaic performance were investigated. The rGO/mp-TiO_2 nanocomposite film reduces interfacial resistance when compared to the mp-TiO_2 film, and hence, it improves charge collection efficiency. This effect significantly increases the short circuit current density and open circuit voltage. The rGO/mp-TiO_2 nanocomposite film with an optimal rGO content of 0.4 vol % shows 18% higher photon conversion efficiency compared with the TiO_2 nanoparticles based perovskite solar cells.

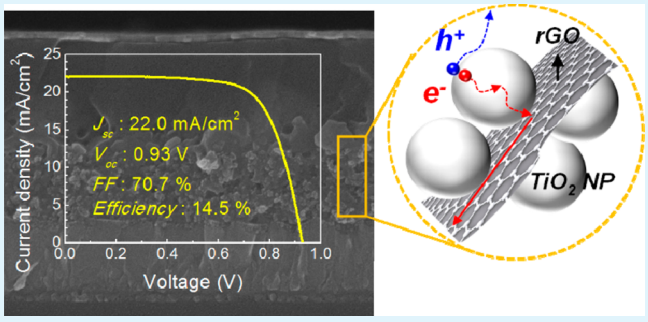

KEYWORDS: *perovskite solar cells, electron transport layer, reduced graphene oxide, TiO_2 nanocomposite, charge collection*

1. INTRODUCTION

Organo lead halide perovskite solar cells have attracted significant research attention because of their exciting improvement in performance to a power conversion efficiency (PCE) of 20.2% in recent years.[1] Such rapid renewal of the world record PCE is largely attributed to the unique properties of the perovskite material: high light absorption coefficient (>10^4 cm^{-1}),[2,3] long charge diffusion length (>1 μm),[4] high charge carrier mobility (25 $cm^2/(V\ s)$),[5] and suitable and adjustable band gap.[6]

Currently, two types of architectures for perovskite solar cells have been adopted. One is a mesostructured solar cell with a mesoporous (mp) electron transport layer (ETL) composed of semiconducting metal oxides (TiO_2, ZnO_2, and so on). The other is a p−i−n or p−n junction planar structured solar cell without the mp-ETL.[7] In particular, for the mesostructured cells, solution-processed $CH_3NH_3PbI_3$ (MALI) exhibits electron and hole diffusion lengths of approximately 130 and 100 nm, respectively.[4,8] Edri et al. recently demonstrated that the hole diffusion length is longer than the electron diffusion length in TiO_2 based ETL through the use of the electron beam induced current (EBIC) imaging method.[9] For the mp-ETL, TiO_2 nanoparticles are typically employed. However, charge recombination in the mp-TiO_2 based ETL is still one of the critical factors that hinder electron transport owing to grain boundary scattering. This limits further improvement in energy conversion efficiency. Therefore, improving charge transport has gained considerable interest. For the mesostructured cells, a number of efforts have been made to facilitate charge transport by employing modified TiO_2 or new nanomaterials, such as aliovalent substitutions of Y^{3+}, Al^{3+}, or Nb^{5+} into TiO_2[10−12] or branched anatase TiO_2 nanowires (ATNWs), TiO_2 nanorods (NRs), or ZnO NRs.[13−15]

On the other hand, graphene (GR) has a remarkably high electron mobility with a Fermi velocity of 10^6 ms^{-1}, good stability, and high transparency at room temperature, making it a suitable substitute to improve the overall conversion efficiency of energy devices such as batteries, supercapacitors, and photoelectrochemical cells.[16−19] In particular, reduced graphene oxide (rGO) has been widely employed to improve the device performances for biosensors,[20,21] memories,[22,23] transistors,[24] and solar cells.[25−29] Several studies have already

Received: July 9, 2015
Accepted: October 7, 2015
Published: October 7, 2015

DOI: 10.1021/acsami.5b06171
ACS Appl. Mater. Interfaces 2015, 7, 23521−23526

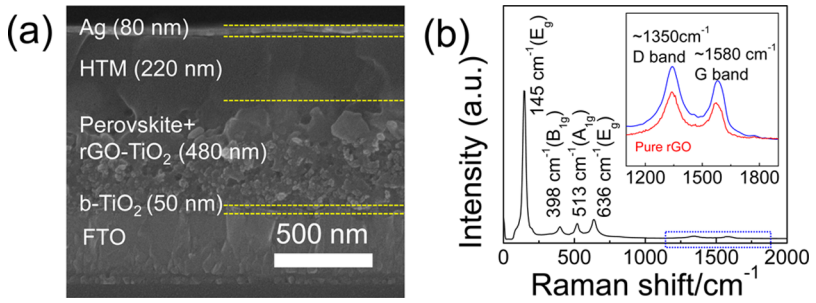

Figure 1. (a) Cross-sectional field emission scanning electron microscopy (FESEM) of 0.4 vol % rGO/mp-TiO_2 nanocomposite based perovskite solar cell; (b) Raman characterization of rGO/mp-TiO_2 nanocomposite films after 450 °C annealing.

demonstrated that rGO (or GR)-semiconductor nanocomposites were an effective additive for boosting the charge collection properties in dye-sensitized solar cells (DSSCs), photocatalysis in which the rGO (or GR) provides a direct pathway for charge transport, and collection in the rGO-TiO_2 (or GR) nanocomposite.[25−27,30−33] More recently, Wang et al. reported that a rGO-TiO_2 composite based blocking layer can reduce the energy barrier and series resistance between TiO_2 and fluorine-doped SnO_2 (FTO) in planar structured solar cells.[34]

Herein, we demonstrate a performance improvement of the mesostructured perovskite solar cell by employing rGO/mp-TiO_2 nanocomposite as the ETL. The influence of the rGO and its concentration on the photovoltaic performance of perovskite solar cells was systematically investigated by electrochemical impedance spectroscopy and transient measurements. We show that the rGO/mp-TiO_2 nanocomposite, compared to the mp-TiO_2 nanoparticles, reduces interfacial resistance and thus improves charge collection efficiency. Consequently, the rGO/mp-TiO_2 nanocomposite for the mesostructured perovskite solar cells exhibited an optimal PCE of 14.5%.

2. EXPERIMENTAL SECTION

Preparation of the rGO-TiO_2 Nanocomposite. In a typical procedure, the rGO was synthesized by a modified Hummers' method.[35] In brief, graphite powder (2 g) was mixed with sulfuric acid (67 mL) and sodium nitrate (1.52 g). Next, potassium permanganate (9 g) was slowly added to the mixture in an ice bath. After 5 days of stirring, the brown mixture was washed 10 times with 5% sulfuric acid solution and water, and then it was centrifuged. rGO was prepared by the addition of hydrazine to the graphene oxide solution. This solution was stirred in an oil bath at 90 °C for 4 h. After it turned black, the dispersion was filtered by vacuum filtration and dried under reduced pressure overnight (Supporting Information (SI) Figures S1 and S2).

For the preparation of the rGO-TiO_2 slurry, we have prepared rGO-ethanol solution first and then it was added into a separately prepared TiO_2 slurry (0.225 g/mL) with various vol % (0, 0.12, 0.22, and 0.56 mg with 0, 0.2, 0.4, and 1.0 vol %, respectively) to minimize aggregation.

Fabrication of the Perovskite Solar Cells. The TiO_2 blocking layers (b-TiO_2) were prepared by sequentially spin coating and drying (120 °C for 10 min) 0.15 and 0.3 M titanium diisopropoxide bis(acetylacetonate) (75 wt % in isopropanol, Sigma-Aldrich) solutions in 1-butanol (99.8%, Sigma-Aldrich), respectively. This was followed by annealing at 500 °C for 30 min. The b-TiO_2/ FTO substrate was immersed in 0.05 M aqueous $TiCl_4$ solution at 70 °C for 30 min. Then, the substrate was rinsed with deionized (DI) water, dried by nitrogen blowing, and annealed at 500 °C for 15 min. The rGO/mp-TiO_2 nanocomposite film was then spin coated onto the b-TiO_2/FTO substrate using prepared slurries and annealed at 450 °C in air for 45 min. There was no notable change in the film morphology and porosity (Supporting Information Figure S3). The perovskite layer was coated onto the prepared rGO/mp-TiO_2 nanocomposite/b-TiO_2/FTO substrate by a sequential deposition of PbI_2 (1.0 M, in dimethylformamide) and CH_3NH_3I (10 mg mL^{-1} MAI, in 2-propanol).[36] MAI was synthesized by a reported procedure.[37] Next, 20 μL of hole transport material (HTM) was deposited by spin coating at 4000 rpm for 40 s. The HTM solution was prepared by mixing 72 mg mL^{-1} spiro-MeOTAD, 17.6 μL of *tert*-butylpyridine, and 28.8 μL of bis(trifluoromethane) sulfonamide lithium salt (Li-TFSI) solution (180 mg in 0.5 mL acetonitrile) in 1 mL cof hlorobenzene. Finally, 80 nm thick silver electrodes were deposited using thermal evaporation.

Measurements and Characterization. The surface morphologies were investigated using field emission scanning electron microscopy (FESEM, JEOL, JSM-7600F). Crystal structures were analyzed using micro-Raman spectroscopy (WITec alpha 300M). Work functions of rGO were analyzed and determined using ultraviolet photoemission spectroscopy (UPS, Thermo Fisher Scientific Co., theta probe base system). The resistivity of the films were measured by Hall measurement (Ecopia, HMS-3300) at room temperature. The transmittance of the rGO/mp-TiO_2 nanocomposite films and the absorbance and reflectance of the perovskite/rGO/mp-TiO_2 nanocomposite films were measured by means of ultraviolet visible (UV/vis) spectroscopy (PerkinElmer, Lamda 35). The photovoltaic performances of the cells were measured using a potentiostat (CHI660, CHI instrument) under AM 1.5 conditions as simulated by a solar simulator (Oriel Sol 3A class AAA, Newport). The $J-V$ curves were measured at 0.05 V s^{-1} scan rate with an active area of 0.14 cm^2. The time constant for the photogenerated electron recombination (τ_R) was measured using a transient photocurrent−voltage spectroscopy setup, which is described elsewhere.[38] The incident photon to current conversion efficiency (IPCE) was measured using an IPCE measurement system (PV Measurements).

3. RESULTS AND DISCUSSION

Figure 1a shows a cross-sectional SEM image of a rGO (0.4 vol %)/mp-TiO_2 nanocomposite based perovskite solar cell in which a blocking TiO_2 layers (b-TiO_2) and rGO/mp-TiO_2 nanocomposite film are approximately 50 and 480 nm thick, respectively. The presence of the rGO in the rGO (0.4 vol %)/mp-TiO_2 nanocomposite film was determined by Raman spectroscopy analysis (Figure 1b). The Raman peaks located at 143 (E_g), 199 (E_g), 396 (B_{1g}), 514 (A_{1g}), and 636 cm^{-1} (E_g) are attributed to the anatase TiO_2 phase.[39] The Raman peaks of rGO located at 1350 cm^{-1} (D band) and 1580 cm^{-1} (G band) confirm the existence of rGO in the rGO-TiO_2 nanocomposites. The G band is related to the optical E_{2g} phonons of sp^2 carbon atoms, and the D band corresponds to the breathing mode of the sp^2 atoms in rings. The D band is also a sign of local defects and disorder.[40] The Raman intensity ratio (I_D/I_G) slightly increases from 1.06 (pure rGO) to 1.16 after the annealing with TiO_2 NPs at 500 °C, indicating the rGO/

DOI: 10.1021/acsami.5b06171
ACS Appl. Mater. Interfaces 2015, 7, 23521−23526

Table 1. Resistivity Values of rGO/mp-TiO_2 Nanocomposite Films

	thickness	resistivity (Ω·cm)
TiO_2 NP film	400 ± 10 nm	(3.03 ± 0.005) × 10^5
(0.2 vol %) rGO/mp-TiO_2 film		2.88 ± 0.007 × 10^5
(0.4 vol %) rGO/mp-TiO_2 film		2.58 ± 0.006 × 10^5
(1.0 vol %) rGO/mp-TiO_2 film		4.94 ± 0.004 × 10^4
only rGO film	20 ± 0.7 μm	1.39 ± 0.032 × 10^{-1}

mp-TiO_2 nanocomposite has a slightly higher amount of defects due to conversion of sp^2 to sp^3.

The resistivity of the rGO/mp-TiO_2 nanocomposite film was measured by Hall measurement, for which TiO_2 nanoparticles (NPs) and rGO/mp-TiO_2 nanocomposite films with an average thickness of 400 nm were deposited on a glass substrate. The results are summarized in Table 1. The TiO_2 NPs film (0 vol % rGO) shows a resistivity of 3.03 × 10^5 Ω·cm, which is comparable with a previous report.[41] In the case of rGO/mp-TiO_2 nanocomposite films, the resistivity is reduced to 2.58 × 10^5 Ω·cm at 0.4 vol % rGO, and it is further reduced to 4.94 × 10^4 Ω·cm at 1.0 vol % rGO. The decrease in the resistivity of the rGO/mp-TiO_2 nanocomposites is attributed to the high conductivity (mobility) of the rGO that reduces the interfacial resistance between TiO_2 NPs.[25,34]

Figure 2 compares the representative $J-V$ curves of the mp-TiO_2 NPs and rGO/mp-TiO_2 nanocomposites based perovskite solar cells. The photovoltaic characteristic values for each cell are summarized in Table 2, and the average values, such as short circuit current density (J_{sc}), open circuit voltage (V_{oc}), fill factor (ff), and power conversion efficiency (PCE), are plotted in Supporting Information Figure S4 (standard deviation of measurements from each of the 16 devices). With the addition of the rGO in the mp-TiO_2, the J_{sc} increased from J_{sc} ~ 19.6 mA/cm^2 to J_{sc} ~ 21.0 mA/cm^2 in the 0.4 vol % rGO/mp-TiO_2 nanocomposite. The V_{oc} and ff also increased from 0.86 to 0.91 V and from 66.8 to 70.8% in the 0.4 vol % rGO/mp-TiO_2 nanocomposite, respectively. As the rGO content further increased to 1.0 vol %, the PCE and J_{sc} decreased to 11.7% and 19.3 mA/cm^2, respectively.

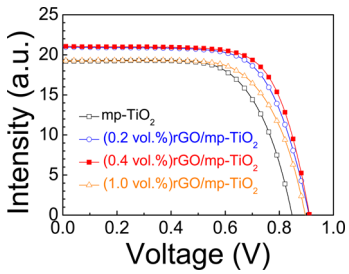

Figure 2. $J-V$ curve of rGO/mp-TiO_2 nanocomposite based perovskite solar cell with varying rGO contents (0.2 vol %, 0.4 vol %, and 1.0 vol %). The mp-TiO_2 NPs based perovskite solar cell is presented as a black line for comparison.

Table 2. $J-V$ Characteristics of rGO/mp-TiO_2 Nanocomposite Based Perovskite Solar Cells with Varying rGO Contents (0.2, 0.4, and 1.0 vol %)

	J_{sc} (mA/cm^2)	V_{oc} (mV)	*FF* (%)	η (%)
TiO_2 NP	19.6	0.86	66.8	11.5
(0.2 vol %) rGO/mp-TiO_2	20.9	0.91	68.5	13.0
(0.4 vol %) rGO/mp-TiO_2	21.0	0.91	70.8	13.5
(1.0 vol %) rGO/mp-TiO_2	19.3	0.89	67.4	11.7

In order to understand the decreased photovoltaic performance at the higher content of rGO, we measured the optical transmittance of the rGO/mp-TiO_2 nanocomposite films as a function of rGO contents (SI Figure S5). Especially for the 1.0 vol % rGO content, the decrease of the transmittance was around 9% compared to that of the mp-TiO_2 only sample. It is widely recognized that rGO can absorb light in the wavelength range of 200−800 nm. Therefore, at the higher amount of the rGO in the rGO/mp-TiO_2, the light absorption by the perovskite absorber reduced, which decreased the photocurrent density from 21.0 mA/cm^2 (for 0.4 vol % rGO) to 19.3 mA/cm^2 (1.0 vol % rGO).(SI Figure S6). Therefore, it is believed that the higher amount of the rGO in rGO/mp-TiO_2 nanocomposite reduces the light harvesting efficiency of the perovskite absorber, which decreases the photocurrent density and solar cell efficiency. Consequently, the maximal photon conversion efficiency (PCE) of the rGO/mp-TiO_2 nanocomposite films was approximately 18% higher than the mp-TiO_2 NPs based perovskite solar cells with the optimal rGO content at 0.4 vol %.

Figure 3a compares the IPCEs of the mp-TiO_2 NPs and rGO/mp-TiO_2 nanocomposite based perovskite solar cells. The rGO/mp-TiO_2 nanocomposite shows higher IPCEs than the mp-TiO_2 NPs in the visible light region. The integrated J_{sc} obtained from the IPCE spectra for the mp-TiO_2 and (0.4 vol %) rGO/mp-TiO_2 nanocomposite based perovskite solar cells were 18.8 and 19.9 mA/cm^2 with maximum IPCEs of 82.99% (at 480 nm) and 88.02% (at 500 nm), respectively. In order to understand these differences in photovoltaic properties, light harvesting efficiency (LHE) and absorbed photon to current conversion efficiency (APCE) were measured and compared. Figure 3b shows the LHE of the mp-TiO_2 and rGO(0.4 vol %)/mp-TiO_2 nanocomposites based perovskite solar cells obtained from the relation LHE = $(1 - R)(1 - 10^{-A})$,[42] where R is the reflectance and A is the absorbance. Even though the rGO/mp-TiO_2 nanocomposite based perovskite solar cell shows slightly lower LHE than the mp-TiO_2 based perovskite solar cell at the longer wavelength, the integrated light absorption values (~84%) in both the mp-TiO_2 and (0.4 vol %)rGO/mp-TiO_2 perovskite solar cells are comparable. The lower LHE of the rGO/mp-TiO_2 nanocomposite is ascribed to the slightly decreased transmittance due to partial absorption by the rGO (Supporting Information Figure S5). More importantly, APCEs (=IPCE/LHE) of the rGO/mp-TiO_2 nanocomposite based perovskite solar cells were ~7% higher than that of the mp-TiO_2 based perovskite solar cells throughout the entire wavelength region. This indicates an improved electron collection property of the rGO/mp-TiO_2 nanocomposite.

The improved charge collection property of the rGO/mp-TiO_2 nanocomposite based perovskite solar cell was further examined using electrochemical impedance spectroscopy (EIS)

DOI: 10.1021/acsami.5b06171
ACS Appl. Mater. Interfaces 2015, 7, 23521−23526

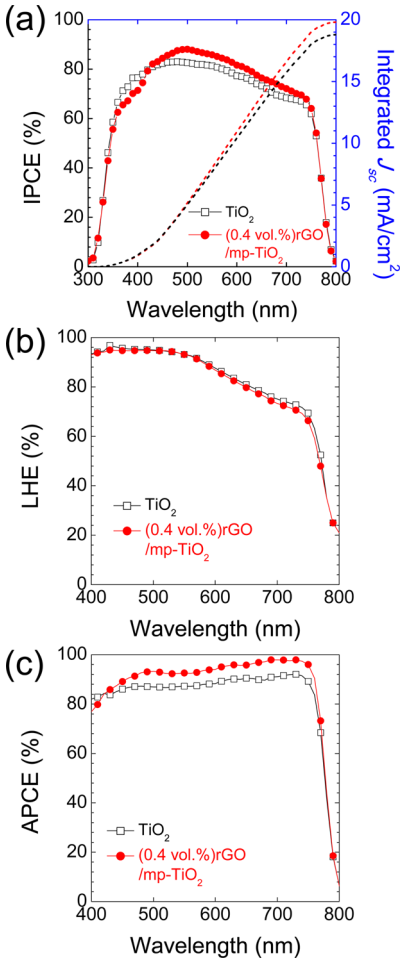

Figure 3. (a) IPCE, (b) LHE, and (c) APCE of rGO/mp-TiO_2 nanocomposite (red line) and mp-TiO_2 NPs (black line) based perovskite solar cells.

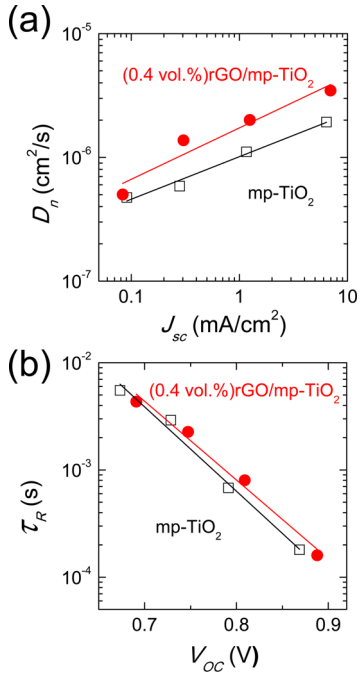

Figure 4. Electron diffusion coefficient (D_n) and charge recombination time (τ_n) of rGO/mp-TiO_2 nanocomposite compared to mp-TiO_2 NPs based perovskite solar cells.

in the frequency range of $1-10^6$ Hz at an open circuit voltage under 1 sun illumination (Supporting Information Figure S7). As already shown in Table 1, the rGO/mp-TiO_2 nanocomposite films show a smaller resistivity compared with that of the mp-TiO_2 NPs. Basically, there are two RC arcs elements representing charge transfer resistance and recombination at TiO_2/perovskite, TiO_2/TiO_2, and rGO/TiO_2 interface. The charge transfer resistance of a rGO/mp-TiO_2 nanocomposite based perovskite solar cell exhibits less recombination than mp-TiO_2 NPs at high frequency (inset of SI Figure S7). Moreover, recombination of rGO/mpTiO_2 nanocomposite based perovskite solar cell at low frequency shows a smaller resistivity compared with that of the mp-TiO_2 NPs. Therefore, these results indicate that the rGO/mp-TiO_2 nanocomposite based perovskite solar cell possesses improved charge collection properties, i.e., enhanced electron transport and reduced charge recombination, versus the mp-TiO_2 NPs based perovskite solar cell.

Finally, to demonstrate the improved charge collection behavior of the rGO/mp-TiO_2 nanocomposite based perovskite solar cells, transient photocurrents and voltages were measured as a function of photocurrent and photovoltage, respectively. Figure 4 shows the electron diffusion coefficients (D_n) and time constants for electron recombination (τ_R) obtained from the transient measurements. In comparison with the mp-TiO_2 NPs based perovskite solar cell, the rGO/mp-TiO_2 nanocomposite based perovskite solar cell shows approximately twice faster D_n. Furthermore, the time constant of the electron recombination in the rGO/mp-TiO_2 composite based cell perovskite solar cell is slightly longer than that in the mp-TiO_2 NPs based perovskite solar cell. These two results support that the rGO/mp-TiO_2 nanocomposite possesses superior charge collection properties, *i.e.*, larger D_n and larger τ_R, for the perovskite solar cells, and it is attributed to the high electron mobility of the rGO.[34] Supporting Information Figure S8 shows an ultraviolet photoelectron spectroscopy (UPS) spectrum of the synthesized rGO, where the energy is calibrated with respect to He I photon energy (21.21 eV). The work function was estimated to be −4.40 eV below vacuum level, which is consistent with the previous reports.[43] To clearly show the charge transfer pathway, the energy band diagram of FTO, TiO_2, rGO, perovskite, and HTM was drawn on the basis of their band gaps and the conduction band edges: TiO_2 (−4.0 eV), perovskite (−3.93 eV), the HOMO level of HTM (spiro-OMeTAD, −5.22 eV), and the work function of rGO (−4.4 eV) (Figure 5). Due to the lower energy level of rGO compared to the conduction band of TiO_2, the photoexcited electrons from TiO_2 and perovskite can be transferred to the rGO. Therefore, the rGO/mp-TiO_2 nanocomposite based perovskite solar cells should provide enhanced charge transport and collection properties. Finally, a best performing rGO/mp-TiO_2 nanocomposite perovskite solar cell is prepared by further controlling film thickness and dispersion of rGO (2-propanol). As shown in Supporting Information Figure S9, the rGO/mp-TiO_2 nanocomposite based perovskite cell achieved J_{sc}, V_{oc}, ff, and PCE values of 22.0 mA/cm^2, 0.93 V, 70.7%, and 14.5%, respectively. Even though the PCE value is not outstanding compared to the previously reported best values,[1] we believe that further modification of the rGO/mp-TiO_2 nanocomposite based ETL with techniques such as

DOI: 10.1021/acsami.5b06171
ACS Appl. Mater. Interfaces 2015, 7, 23521−23526

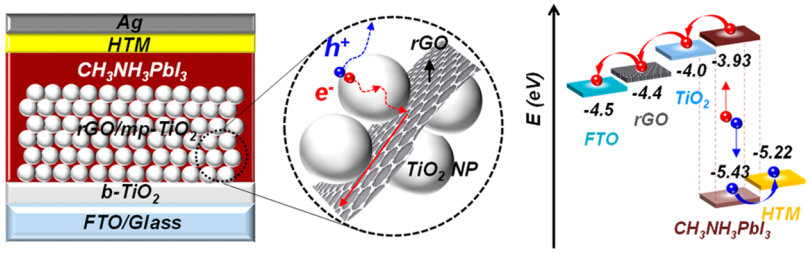

Figure 5. Diagram of rGO/mp-TiO_2 nanocomposite based perovskite solar cells.

surface passivation by atomic layered deposition (ALD) will improve the PCE further by increasing the fill factor.

4. CONCLUSION

In summary, we fabricated an rGO/mp-TiO_2 nanocomposite based electron transport layer for perovskite solar cells. The rGO/mp-TiO_2 nanocomposite based perovskite solar cells exhibited an increase in J_{sc}, ff, and V_{oc} as compared to mp-TiO_2 based perovskite solar cells. The electrochemical impedance spectroscopy analysis and transient studies revealed that the rGO/mp-TiO_2 nanocomposite film has reduced internal resistance and enhanced charge collection, which improves the photovoltaic performance of the rGO/mp-TiO_2 nanocomposite based perovskite solar cell. The optimized perovskite solar cell based on the rGO/mp-TiO_2 nanocomposite showed a higher energy conversion efficiency of 14.5% as compared to the 13.5% of the mp-TiO_2 NPs based perovskite cell. We believe that the introduction of rGO into the TiO_2 based electron transport layer is one of the simplest ways to mitigate large recombination at the TiO_2 grain boundaries, thus improving the charge collection at the TiO_2/TiO_2 or $TiO_2/CH_3NH_3PbI_3$ interface in perovskite solar cells.

■ ASSOCIATED CONTENT

Supporting Information

The Supporting Information is available free of charge on the ACS Publications website at DOI: 10.1021/acsami.5b06171.

SEM image of synthesized rGO, XPS spectra of rGO, top-view SEM images and absorption spectra of desorbed dye in each film, photovoltaic properties of rGO-TiO_2 based solar cells, transmittance of films, Nyquist plots of rGO/mp-TiO_2, UPS of rGO, and $J-V$ curves for best performing solar cells studied, (PDF)

■ AUTHOR INFORMATION

Corresponding Authors

*(I.S.C.) Tel.: +82-31-219-2468. Fax: +82-31-219-1613. E-mail: insuncho@ajou.ac.kr.

*(D.H.Y.) Tel.: +82-31-290-7361. Fax: +82-31-290-7410. E-mail: dhyoon@skku.edu.

*(H.S.J.) Tel.: +82-31-290-7403. Fax: +82-31-290-7410. E-mail: hsjung1@skku.edu.

Author Contributions

#G.S.H. and Y.H.S contributed equally to this work.

Notes

The authors declare no competing financial interest.

■ ACKNOWLEDGMENTS

This work was supported by the National Research Foundation of Korea (NRF) grants funded by the Ministry of Science, ICT & Future Planning (MSIP) of Korea under Contract Nos. NRF-2014R1A4A1008474, NRF-2013R1A2A2A01010027, 2012M3A7B4049967 (Nano.Material Technology Development Program), and 2012M3A6A7054861 (Global Frontier R&D Program on Center for Multiscale Energy System).

■ REFERENCES

(1) Yang, W. S.; Noh, J. H.; Jeon, N. J.; Kim, Y. C.; Ryu, S.; Seo, J.; Seok, S. I. High-Performance Photovoltaic Perovskite Layers Fabricated Through Intramolecular Exchange. *Science* **2015**, *348*, 1234−1237.

(2) De Wolf, S.; Holovsky, J.; Moon, S.-J.; Löper, P.; Niesen, B.; Ledinsky, M.; Haug, F.-J.; Yum, J.-H.; Ballif, C. Organometallic Halide Perovskites: Sharp Optical Absorption Edge and Its Relation to Photovoltaic Performance. *J. Phys. Chem. Lett.* **2014**, *5*, 1035−1039.

(3) Ziang, X.; Shifeng, L.; Laixiang, Q.; Shuping, P.; Wei, W.; Yu, Y.; Li, Y.; Zhijian, C.; Shufeng, W.; Honglin, D.; Minghui, Y.; Qin, G. G. Refractive Index and Extinction Coefficient of CH3NH3PbI3 Studied by Spectroscopic Ellipsometry. *Opt. Mater. Express* **2015**, *5*, 29−43.

(4) Stranks, S. D.; Eperon, G. E.; Grancini, G.; Menelaou, C.; Alcocer, M. J. P.; Leijtens, T.; Herz, L. M.; Petrozza, A.; Snaith, H. J. Electron-Hole Diffusion Lengths Exceeding 1 Micrometer in an Organometal Trihalide Perovskite Absorber. *Science* **2013**, *342*, 341−344.

(5) Kim, H.-S.; Mora-Sero, I.; Gonzalez-Pedro, V.; Fabregat-Santiago, F.; Juarez-Perez, E. J.; Park, N.-G.; Bisquert, J., Mechanism of Carrier Accumulation in Perovskite Thin-Absorber Solar Cells. *Nat. Commun.* **2013**, *4*.224210.1038/ncomms3242

(6) Noh, J. H.; Im, S. H.; Heo, J. H.; Mandal, T. N.; Seok, S. I. Chemical Management for Colorful, Efficient, and Stable Inorganic−Organic Hybrid Nanostructured Solar Cells. *Nano Lett.* **2013**, *13*, 1764−1769.

(7) Kim, H.-S.; Im, S. H.; Park, N.-G. Organolead Halide Perovskite: New Horizons in Solar Cell Research. *J. Phys. Chem. C* **2014**, *118*, 5615−5625.

(8) Xing, G.; Mathews, N.; Sun, S.; Lim, S. S.; Lam, Y. M.; Grätzel, M.; Mhaisalkar, S.; Sum, T. C. Long-Range Balanced Electron- and Hole-Transport Lengths in Organic-Inorganic CH3NH3PbI3. *Science* **2013**, *342*, 344−347.

(9) Edri, E.; Kirmayer, S.; Henning, A.; Mukhopadhyay, S.; Gartsman, K.; Rosenwaks, Y.; Hodes, G.; Cahen, D. Why Lead Methylammonium Tri-Iodide Perovskite-Based Solar Cells Require a Mesoporous Electron Transporting Scaffold (but Not Necessarily a Hole Conductor). *Nano Lett.* **2014**, *14*, 1000−1004.

(10) Qin, P.; Domanski, A. L.; Chandiran, A. K.; Berger, R.; Butt, H.-J.; Dar, M. I.; Moehl, T.; Tetreault, N.; Gao, P.; Ahmad, S.; Nazeeruddin, M. K.; Gratzel, M. Yttrium-Substituted Nanocrystalline TiO2 Photoanodes for Perovskite Based Heterojunction Solar Cells. *Nanoscale* **2014**, *6*, 1508−1514.

(11) Pathak, S. K.; Abate, A.; Ruckdeschel, P.; Roose, B.; Gödel, K. C.; Vaynzof, Y.; Santhala, A.; Watanabe, S.-I.; Hollman, D. J.; Noel, N.; Sepe, A.; Wiesner, U.; Friend, R.; Snaith, H. J.; Steiner, U. Performance and Stability Enhancement of Dye-Sensitized and Perovskite Solar Cells by Al Doping of TiO2. *Adv. Funct. Mater.* **2014**, *24*, 6046−6055.

DOI: 10.1021/acsami.5b06171
ACS Appl. Mater. Interfaces 2015, 7, 23521−23526

(12) Kim, D. H.; Han, G. S.; Seong, W. M.; Lee, J.-W.; Kim, B. J.; Park, N.-G.; Hong, K. S.; Lee, S.; Jung, H. S. Niobium Doping Effects on TiO_2 Mesoscopic Electron Transport Layer-Based Perovskite Solar Cells. *ChemSusChem* **2015**, *8*, 2392−2398.
(13) Wu, W.-Q.; Huang, F.; Chen, D.; Cheng, Y.-B.; Caruso, R. A. Thin Films of Dendritic Anatase Titania Nanowires Enable Effective Hole-Blocking and Efficient Light-Harvesting for High-Performance Mesoscopic Perovskite Solar Cells. *Adv. Funct. Mater.* **2015**, *25*, 3264−3272.
(14) Kim, H.-S.; Lee, J.-W.; Yantara, N.; Boix, P. P.; Kulkarni, S. A.; Mhaisalkar, S.; Grätzel, M.; Park, N.-G. High Efficiency Solid-State Sensitized Solar Cell-Based on Submicrometer Rutile TiO2 Nanorod and CH3NH3PbI3 Perovskite Sensitizer. *Nano Lett.* **2013**, *13*, 2412−2417.
(15) Son, D.-Y.; Im, J.-H.; Kim, H.-S.; Park, N.-G. 11% Efficient Perovskite Solar Cell Based on ZnO Nanorods: An Effective Charge Collection System. *J. Phys. Chem. C* **2014**, *118*, 16567−16573.
(16) Huang, X.; Zeng, Z.; Fan, Z.; Liu, J.; Zhang, H. Graphene-Based Electrodes. *Adv. Mater.* **2012**, *24*, 5979−6004.
(17) Huang, X.; Qi, X.; Boey, F.; Zhang, H. Graphene-based composites. *Chem. Soc. Rev.* **2012**, *41*, 666−686.
(18) Radich, J. G.; Krenselewski, A. L.; Zhu, J.; Kamat, P. V. Is Graphene a Stable Platform for Photocatalysis? Mineralization of Reduced Graphene Oxide With UV-Irradiated TiO2 Nanoparticles. *Chem. Mater.* **2014**, *26*, 4662−4668.
(19) Lightcap, I. V.; Kamat, P. V. Graphitic Design: Prospects of Graphene-Based Nanocomposites for Solar Energy Conversion, Storage, and Sensing. *Acc. Chem. Res.* **2013**, *46*, 2235−2243.
(20) He, Q.; Sudibya, H. G.; Yin, Z.; Wu, S.; Li, H.; Boey, F.; Huang, W.; Chen, P.; Zhang, H. Centimeter-Long and Large-Scale Micropatterns of Reduced Graphene Oxide Films: Fabrication and Sensing Applications. *ACS Nano* **2010**, *4*, 3201−3208.
(21) Wang, Z.; Zhou, X.; Zhang, J.; Boey, F.; Zhang, H. Direct Electrochemical Reduction of Single-Layer Graphene Oxide and Subsequent Functionalization with Glucose Oxidase. *J. Phys. Chem. C* **2009**, *113*, 14071−14075.
(22) Liu, J.; Yin, Z.; Cao, X.; Zhao, F.; Lin, A.; Xie, L.; Fan, Q.; Boey, F.; Zhang, H.; Huang, W. Bulk Heterojunction Polymer Memory Devices with Reduced Graphene Oxide as Electrodes. *ACS Nano* **2010**, *4*, 3987−3992.
(23) Liu, J.; Lin, Z.; Liu, T.; Yin, Z.; Zhou, X.; Chen, S.; Xie, L.; Boey, F.; Zhang, H.; Huang, W. Multilayer Stacked Low-Temperature-Reduced Graphene Oxide Films: Preparation, Characterization, and Application in Polymer Memory Devices. *Small* **2010**, *6*, 1536−1542.
(24) He, Q.; Wu, S.; Gao, S.; Cao, X.; Yin, Z.; Li, H.; Chen, P.; Zhang, H. Transparent, Flexible, All-Reduced Graphene Oxide Thin Film Transistors. *ACS Nano* **2011**, *5*, 5038−5044.
(25) Yang, N.; Zhai, J.; Wang, D.; Chen, Y.; Jiang, L. Two-Dimensional Graphene Bridges Enhanced Photoinduced Charge Transport in Dye-Sensitized Solar Cells. *ACS Nano* **2010**, *4*, 887−894.
(26) Song, J.; Yin, Z.; Yang, Z.; Amaladass, P.; Wu, S.; Ye, J.; Zhao, Y.; Deng, W.-Q.; Zhang, H.; Liu, X.-W. Enhancement of Photogenerated Electron Transport in Dye-Sensitized Solar Cells with Introduction of a Reduced Graphene Oxide−TiO2 Junction. *Chem. - Eur. J.* **2011**, *17*, 10832−10837.
(27) Ng, Y. H.; Lightcap, I. V.; Goodwin, K.; Matsumura, M.; Kamat, P. V. To What Extent Do Graphene Scaffolds Improve the Photovoltaic and Photocatalytic Response of TiO2 Nanostructured Films? *J. Phys. Chem. Lett.* **2010**, *1*, 2222−2227.
(28) Yin, Z.; Sun, S.; Salim, T.; Wu, S.; Huang, X.; He, Q.; Lam, Y. M.; Zhang, H. Organic Photovoltaic Devices Using Highly Flexible Reduced Graphene Oxide Films as Transparent Electrodes. *ACS Nano* **2010**, *4*, 5263−5268.
(29) Yin, Z.; Wu, S.; Zhou, X.; Huang, X.; Zhang, Q.; Boey, F.; Zhang, H. Electrochemical Deposition of ZnO Nanorods on Transparent Reduced Graphene Oxide Electrodes for Hybrid Solar Cells. *Small* **2010**, *6*, 307−312.
(30) Yang, M.-Q.; Zhang, N.; Pagliaro, M.; Xu, Y.-J. Artificial Photosynthesis Over Graphene−Semiconductor Composites. Are We Getting Better? *Chem. Soc. Rev.* **2014**, *43*, 8240−8254.
(31) Zhang, N.; Zhang, Y.; Xu, Y.-J. Recent Progress on Graphene-Based Photocatalysts: Current Status and Future Perspectives. *Nanoscale* **2012**, *4*, 5792−5813.
(32) Zhang, Y.; Tang, Z.-R.; Fu, X.; Xu, Y.-J. TiO2− Graphene Nanocomposites for Gas-Phase Photocatalytic Degradation of Volatile Aromatic Pollutant: is TiO2− Graphene Truly Different from Other TiO2− Carbon Composite Materials? *ACS Nano* **2010**, *4*, 7303−7314.
(33) Zhang, Y.; Tang, Z.-R.; Fu, X.; Xu, Y.-J. Engineering the Unique 2D Mat of Graphene to Achieve Graphene-TiO2 Nanocomposite for Photocatalytic Selective Transformation: What Advantage does Graphene have over its Forebear Carbon Nanotube? *ACS Nano* **2011**, *5*, 7426−7435.
(34) Wang, J. T.-W.; Ball, J. M.; Barea, E. M.; Abate, A.; Alexander-Webber, J. A.; Huang, J.; Saliba, M.; Mora-Sero, I.; Bisquert, J.; Snaith, H. J.; Nicholas, R. J. Low-Temperature Processed Electron Collection Layers of Graphene/TiO2 Nanocomposites in Thin Film Perovskite Solar Cells. *Nano Lett.* **2014**, *14*, 724−730.
(35) Kumar, N. A.; Gambarelli, S.; Duclairoir, F.; Bidan, G.; Dubois, L. Synthesis of High Quality Reduced Graphene Oxide Nanosheets Free of Paramagnetic Metallic Impurities. *J. Mater. Chem. A* **2013**, *1*, 2789−2794.
(36) Burschka, J.; Pellet, N.; Moon, S.-J.; Humphry-Baker, R.; Gao, P.; Nazeeruddin, M. K.; Gratzel, M. Sequential Deposition as a Route to High-Performance Perovskite-Sensitized Solar Cells. *Nature* **2013**, *499*, 316−319.
(37) Kim, H.-S.; Lee, C.-R.; Im, J.-H.; Lee, K.-B.; Moehl, T.; Marchioro, A.; Moon, S.-J.; Humphry-Baker, R.; Yum, J.-H.; Moser, J. E.; Grätzel, M.; Park, N.-G. Lead Iodide Perovskite Sensitized All-Solid-State Submicron Thin Film Mesoscopic Solar Cell with Efficiency Exceeding 9%. *Sci. Rep.* **2012**, *2*, 501.
(38) Kim, M.-J.; Lee, C.-R.; Jeong, W.-S.; Im, J.-H.; Ryu, T. I.; Park, N.-G. Unusual Enhancement of Photocurrent by Incorporation of Brönsted Base Thiourea into Electrolyte of Dye-Sensitized Solar Cell. *J. Phys. Chem. C* **2010**, *114*, 19849−19852.
(39) Ohsaka, T.; Izumi, F.; Fujiki, Y. Raman spectrum of anatase, TiO2. *J. Raman Spectrosc.* **1978**, *7*, 321−324.
(40) Ferrari, A. C.; Meyer, J. C.; Scardaci, V.; Casiraghi, C.; Lazzeri, M.; Mauri, F.; Piscanec, S.; Jiang, D.; Novoselov, K. S.; Roth, S.; Geim, A. K. Raman Spectrum of Graphene and Graphene Layers. *Phys. Rev. Lett.* **2006**, *97*, 187401.
(41) Pawar, S.; Patil, S.; Chougule, M.; Raut, B.; Jundale, D.; Patil, V. Polyaniline: TiO_2 Nanocomposites: Synthesis and Characterization. *Arch. Appl. Sci. Res.* **2010**, *2*, 194−201.
(42) Agrios, A. G.; Hagfeldt, A. Low-temperature TiO2 Films for Dye-sensitized Solar Cells: Factors Affecting Energy Conversion Efficiency. *J. Phys. Chem. C* **2008**, *112*, 10021−10026.
(43) Lee, J. S.; You, K. H.; Park, C. B. Highly Photoactive, Low Bandgap TiO2 Nanoparticles Wrapped by Graphene. *Adv. Mater.* **2012**, *24*, 1084−1088.

DOI: 10.1021/acsami.5b06171
ACS Appl. Mater. Interfaces 2015, 7, 23521−23526